Robust Increases in Midlatitude Static Stability in Simulations of Global Warming

Dargan M. W. Frierson

UCAR/University of Chicago

October 2006

Abstract

We examine changes in the static stability of the midlatitude troposphere in simulations of global warming using 21 coupled climate models in the AR4 archive. The dry static stability within the midlatitudes exhibits a robust increase in the simulations, with upper tropospheric warming outpacing the lower troposphere by approximately 2 K. The increase in stability is especially evident in the summer season, and is more prominent in the Southern Hemisphere than in the Northern. The moist static stability is largely unchanged, on the other hand, showing that moist convection plays a dominant role in determining the temperature structure of the midlatitudes. We compare bulk measures of the stability with changes in meridional gradients for each individual model simulation, and find that moist theories work well in predicting the stability with the primary exception of the Northern Hemisphere summer, where enhanced surface warming over land reduces the increase in stability.

1. Introduction

Static stability is among the most fundamental quantities describing the state of the atmosphere. Equivalent to the vertical temperature structure of the atmosphere, the static stability determines the buoyancy frequency of dry perturbations in the vertical, the speed of gravity waves, and the magnitude of the greenhouse effect. In the midlatitudes in particular, the static stability is a key ingredient to any theory of the general circulation.

The determination of the static stability of the tropical troposphere is relatively well understood: there moist convection occurs over warm waters, and sets the upper tropospheric temperatures. The temperature structure there is thus approximately given by the moist adiabat (Xu and Emanuel 1989). The moist adiabatic structure then results in upper tropospheric amplification of global warming within the tropics, and hence a more stable troposphere in terms of dry stability with increases in temperature. In observations, there remain discrepancies between model predictions and observations in the tropics, but large observational uncertainties make it difficult to determine whether this theoretical understanding is flawed (CCSP 2006).

In the midlatitudes, on the other hand, the determination of the static stability is much less well understood from a theoretical perspective. Early theories relied on dry baroclinic eddy dynamics to understand midlatitude static stability (Stone (1972); Held (1982)). Theories such as Stone (1978) and Held (1982) derive a constraint that relates the static stability to meridional temperature gradients:

$$\theta_z \sim \frac{f}{H\beta}\theta_y. \tag{1}$$

with θ the potential temperature, f and β the Coriolis parameter and its gradient, and H some depth scale. However recent studies have shown that the detailed predictions of these theories are not born out in a general circulation model (GCM) (Thuburn and Craig 1997) or in reanalysis data

(Juckes 2000). Recently, instead, focus has been turned to moist convection as being important in the determination of the midlatitude stability, as it is in the tropics (Juckes 2000). In this argument, moist convection occurs within the warm cores of baroclinic eddies (as it is observed to in Emanuel (1988)), setting minimum stability. The net moist stability of the midlatitudes is then determined by the standard deviation of the surface equivalent potential temperature, which can be related to meridional gradients through mixing length-like closures. The end result relates the moist stability to surface equivalent potential temperature gradients (Frierson et al. 2006a):

$$\theta_{ez} \sim \theta_{ey} \tag{2}$$

where θ_e is the equivalent potential temperature.

The predictions of Eqn. 2 have been found to be accurate for a simplified moist general circulation model (Frierson et al. 2006a). Eqn. 2 predicts an increase in dry stability with moisture content and thus with the mean temperature of the atmosphere; in this sense the argument could additionally be used to explain the increase in static stability with sea surface temperature (SST) seen in the aquaplanet full GCM simulations of Caballero and Langen (2005).

Simulations of global warming provide a unique test of the determination of the midlatitude static stability. The temperature changes in the more extreme scenarios can be significantly larger than interannual variability within observations, but clearly not outside the range of realism. Further, using the best models of various climate modelling groups around the world and their associated parameterizations of clouds, convection, and other physics provides a measure of robustness to physical parameterization that is impossible with a single model. In this paper we analyze the changes in bulk (vertically integrated) measures of the static stability in global warming scenarios in 21 coupled GCM's, and compare with the various theories listed above.

2. Description of Model Simulations

We analyze data from 21 coupled GCM's used in the Intergovernmental Panel on Climate Change (IPCC) Fourth Assessment Report (AR4). The data was archived by the Program for Climate Model Diagnosis and Intercomparison (PCMDI), and is available from https://esg.llnl.gov:8443/index.jsp. The models utilized, in order of their archived meridional resolution from high to low, are: MIROC3.2(hires); UKMO-HadGEM1; CCSM3; CSIRO-Mk3.0, ECHAM5/MPI-OM; GFDL-CM2.0, GFDL-CM2.1; IPSL-CM4, UKMO-HadCM3; BCCR-BCM2.0, CGCM3.1(T63), CNRM-CM3, FGOALS-g1.0, MIROC3.2(medres), MRI-CGCM2.3.2, PCM; GISS-AOM; CGCM3.1(T47); GISS-EH, GISS-ER, INM-CM3.0. Documentation for the models is available at http://www-pcmdi.llnl.gov/ipcc/model_documentation/ipcc_model_documentation.php.

We compare the Climate of the 20th Century (20C3M) scenario with the SRESA1B scenario, which stabilizes at 720 ppm of CO2. We compare 18 years of the 20C3M scenario, from September 1981 to August 1999, with 18 years of the SRESA1B scenario, from September 2081 to August 2099. This follows to a large extent the analysis procedure used by Yin (2005) to study the changes in the latitude of the storm tracks in the AR4 models. We utilize the monthly mean datasets in the following analysis. Simulations are interpolated to T42 (2.8 degree) horizontal resolution to construct the multi-model ensemble mean diagnostics below. Averages are omitted if over 50% of the data is missing (e.g., if over half of the points at a particular latitude and pressure level are underground). For surface averages, we omit points where the surface is above 850 hPa.

3. Results

In Figure 1 we plot the change in multi-model ensemble mean, zonal mean potential temperature (θ) change for the A1B scenario minus the 20C3M scenario. The mean for the months of December/January/February are given in Figure 1a, and the mean for June/July/August are given in Figure 1b. Familiar features dominate these plots: polar amplification in the Northern Hemisphere (NH) winter primarily confined to the lower troposphere, stratospheric cooling, and increases in tropical static stability associated with the moist adiabat. In addition to these features, there is a clear increase in the static stability within the midlatitudes: between 30 and 60 degrees, the upper troposphere warms more than the lower troposphere by an average of approximately 2 K. The increase in midlatitude stability occurs within both hemispheres and in both seasons, but the summer hemispheres show larger increases. Additionally, the increases are greater in the Southern Hemisphere (SH) when compared with the same season in the NH.

When differenced between the surface and 400 hPa (we choose 400 hPa as the upper level for averaging the static stability to avoid stratospheric cooling and changes in tropopause height), the increase in stability occurs at all latitudes in NH summer, SH summer, and SH winter. In NH winter, there is polar amplification near the surface which extends from the pole past 50 degrees, and the bulk static stability only increases from the equator up to 56 degrees. When averaged with latitude between 30 and 60 degrees (we average between 30 and 60 degrees to avoid the Hadley circulation and the latitudes of significant polar amplification), the increases in bulk stability are 0.8 K, 2.2 K, 2.4 K, and 2.9 K for NH winter, SH winter, NH summer, and SH summer, respectively. Examining the longitudinal distribution of the stability changes indicates that the increase in stability is significantly less over land in both hemispheres and seasons (not shown).

To explain the increase in dry stability, we next analyze the changes in moist stability by plot-

ting the change in saturated equivalent potential temperature, $\theta_e^* = \theta\ exp(\frac{L_v q^*}{c_p T})$, with q^* the saturation specific humidity and L_v the latent heat of vaporization, in Figure 2. For a moist adiabat, θ_e^* is constant with height above the lifting condensation level; the vertical profile of θ_e^* above the boundary layer thus gives the moist stability of the atmosphere in the same way as the vertical profile of θ gives the dry stability. As expected from the dominance of moist convection within the tropics, the tropical troposphere remains relatively neutral to moist convection in both seasons, as indicated by the predominantly vertical nature of the θ_e^* contours within this region (we explain the deviations from the moist adiabat in the next paragraph). The verticality of the θ_e^* contours extends well into the midlatitudes however. The increase in saturated equivalent potential temperature occurs in a manner that is approximately constant with height, with the primary exception being where polar amplification is occuring. Throughout much of the troposphere, in fact, the vertical temperature structure of the atmosphere can be explained to first order by approximately constant change in saturated equivalent potential temperature with height.

There are prominent deviations from neutral moist stability within Figure 2. Even in the tropics the moist stability decreases somewhat, especially in the NH summer. Much of this can be attributed to increases in the surface temperatures over continental interiors. Land warms more than ocean in the A1B scenario, especially in summer, but this preferential warming over the drier land surfaces does not penetrate into the upper troposphere along with the moist adiabat due to lack of surface moisture. Supplementary Figure 1 depicts the change in saturated equivalent potential temperature averaged over ocean only, which eliminates much of the decrease in moist stability. Further, at least part of the moist stability decrease which remains in the supplementary figure can be attributed to regions just adjacent to the land surfaces.

The moist stability changes in midlatitudes as well. In the SH, the moist stability increases slightly in both seasons, primarily in the summer. In the NH, on the other hand, the moist stability

decreases in both seasons. Defining a bulk moist stability as θ_e^* at 400 hPa minus the surface θ_e, and averaging this measure between 30 and 60 degrees, we find that the bulk moist stability changes are -0.6 K, 0.7 K, -0.3 K, and 1.2 K for NH winter, SH winter, NH summer, and SH summer, respectively.

To compare with the theories outlined in the introduction, we plot the bulk stability changes within 20 of the models against the changes in meridional gradients of θ and θ_e in Figure 3. The CSIRO model was omitted from this analysis due to incomplete surface data in the A1B scenario. Each mark on these plots represents one season (DJF, MAM, JJA, or SON) in the NH or SH of one model simulation. Since the height for calculation of the meridional gradients varies in the dry baroclinic theories described in the introduction, we plot dry stability changes against surface temperature in Figure 3a, and midtropospheric temperature in Figure 3b. We assume f, β, and H to be fixed in these calculations. One can see in Figures 3a and 3b that the bulk dry stability increases in 158 of the 160 model seasons. The two exceptional cases, both in NH winter, experience the farthest penetration of polar amplification into midlatitudes, which leads to the reduced stability.

From Figure 3a it is clear that while the dry stability and surface temperature are correlated, the increases in stability occur for the most part with decreases in the surface temperature gradient. Equation 1 requires an increase in temperature gradient for increases in stability to occur; thus we must reject the theory of Equation 1 using the surface temperature gradient. In Figure 3b, we compare the increases in dry stability with the meridional potential temperature gradient at 500 hPa, which provides a test for theories such as Held (1982). Here the increases in stability are more often associated with an increase in temperature gradients, as predicted by the theory. But in this case the correlation between the two variables is significantly lower. Particularly the NH summer deviates from predictions with the increases in dry stability often accompanied by decreases in the meridional temperature gradients. SH summer and the fall seasons in both hemispheres also

deviate from predictions significantly. While it is plausible that moist convection controls the static stability only in these seasons by setting a larger stability than would occur otherwise with dry baroclinic adjustment, a more likely theory, as we explain next, is that moist convection contributes to the stability in all hemispheres as described by Juckes (2000).

We test these moist theories in the form of Eqn. 2 in Figure 3c, plotting the change in moist stability (θ_e^* at 400 hPa minus surface θ_e) versus change in the meridional gradient of θ_e at the surface. These quantities are roughly correlated for all points, with higher correlations in the SH. There, we argue, the ample availability of moisture from the predominantly ocean surface allows moist convection to determine the zonally averaged stability. The predictions of Eqn. 2 are less accurate in the NH, especially within summer, where the moist stability exhibits a decrease despite increases in meridional gradients of θ_e. This indicates that convection is actually less dominant in the NH summer, in contrast to the possible scenario presented in the previous paragraph. The reduced importance of convection in the NH is due to the greater amount of land within this hemisphere, which limits the availability of moisture and has enhanced surface warming. Supplementary Figure 2, which shows the latitudinal structure of the moist stability change, shows that the primary reduction in moist stability is over land or downwind of the continents. A more complete analysis of the vertical structure of temperature changes as a function of latitude and longitude in these models, in concert with studies of the effect of land on static stability in simpler settings, is warranted to better understand the stability changes in the NH.

4. Conclusions

We have examined a robust increase in the midlatitude dry static stability in IPCC AR4 simulations of global warming. The dry stability within the midlatitudes increases largely in accordance with

the moist adiabat, and changes in the moist stability can be related to changes in θ_e at the surface, as in the theory of Juckes (2000), which takes moist convection within the warm areas of baroclinic eddies as important in determining the static stability in midlatitudes. Although the dry stability still increases there, Juckes' theory performs worst within the NH, where the limited availability of moisture over land surfaces reduces the moist stability. The SH hence has more stability increase than the NH.

Two effects can be cited for the preferential increase of the summer dry stability, which both relate to the increased moisture content in that season: first, the increased dry stability of the moist adiabat with higher temperatures, and second, the increased meridional θ_e gradients, which is dominated by increases in moisture content as well.

This study connects the changes in static stability in GCM simulations of global warming with theoretical work on the subject. We have examined some of the implications of changes in midlatitude static stability on eddy length scales, eddy kinetic energy, the poleward shift of the storm tracks, and poleward energy fluxes within an idealized moist GCM in Frierson et al. (2006a) and Frierson et al. (2006b). With further work on this subject on the theoretical side, the GCM analysis side, and the observational side, the changes in midlatitude static stability may provide us with another theoretically-based fingerprinting technique for the detection of human-induced climate change, as in Santer et al. (1996).

5. Acknowledgements

We acknowledge the international modeling groups for providing their data for analysis, the Program for Climate Model Diagnosis and Intercomparison (PCMDI) for collecting and archiving the model data, the JSC/CLIVAR Working Group on Coupled Modelling (WGCM) and their Coupled Model Intercomparison Project (CMIP) and Climate Simulation Panel for organizing the model data analysis activity, and the IPCC WG1 TSU for technical support. The IPCC Data Archive at Lawrence Livermore National Laboratory is supported by the Office of Science, U.S. Department of Energy. We thank Pablo Zurita-Gotor and Raymond Pierrehumbert for helpful comments on the manuscript. This work is supported by the NOAA Climate and Global Change Postdoctoral Fellowship, administered by the University Corporation for Atmospheric Research.

References

Caballero, R. and P. L. Langen: 2005, The dynamic range of poleward energy transport in an atmospheric general circulation model. *Geophys. Res. Lett.*, **32**, L2705, doi:10.1029/2004GL021581.

CCSP: 2006, Temperature Trends in the Lower Atmosphere: Steps for Understanding and Reconciling Differences. Technical report, Climate Change Science Program and the Subcommittee on Global Change Research, Washington, DC.

Emanuel, K. A.: 1988, Observational evidence of slantwise convective adjustment. *Mon. Wea. Rev.*, **116**, 1805–1816.

Frierson, D. M. W., I. M. Held, and P. Zurita-Gotor: 2006a, A gray-radiation aquaplanet moist GCM. Part I: Static stability and eddy scale. *In press, J. Atmos. Sci.*.

— 2006b, A gray-radiation aquaplanet moist GCM. Part II: Energy transports in altered climates. *In press, J. Atmos. Sci.*.

Held, I. M.: 1982, On the height of the tropopause and the static stability of the troposphere. *J. Atmos. Sci.*, **39**, 412–417.

Juckes, M. N.: 2000, The static stability of the midlatitude troposphere: The relevance of moisture. *J. Atmos. Sci.*, **57**, 3050–3057.

Santer, B. D., K. E. Taylor, T. M. L. Wigley, T. C. Johns, P. D. Jones, D. J. Karoly, J. F. B. Mitchell, A. H. Oort, J. E. Penner, V. Ramaswamy, M. D. Schwarzkopf, R. J. Stouffer, and S. Tett: 1996, A search for human influences on the thermal structure of the atmosphere. *Nature*, **382**, 39–46.

Stone, P. H.: 1972, A simplified radiative-dynamical model for the static stability of rotating atmospheres. *J. Atmos. Sci*, **29**, 405–418.

— 1978, Baroclinic adjustment. *J. Atmos. Sci*, **35**, 561–571.

Thuburn, J. and G. C. Craig: 1997, GCM tests of theories for the height of the tropopause. *J. Atmos. Sci.*, **54**, 869–882.

Xu, K.-M. and K. A. Emanuel: 1989, Is the tropical atmosphere conditionally unstable? *Mon. Wea. Rev.*, **117**, 1471–1479.

Yin, J. H.: 2005, A consistent poleward shift of the storm tracks in simulations of 21st century climate . *Geophys. Res. Lett.*, **32**, L18701, doi:10.1029/2005GL023684.

List of Figures

1 Change in potential temperature (K) for the ensemble mean over all models, DJF (left) and JJA (right), scenario A1B minus scenario 20C3M. Areas with mean cooling (in the polar stratosphere) are not colored. 13

2 Change in saturated equivalent potential temperature (K) for the ensemble mean over all models, DJF (left) and JJA (right), scenario A1B minus scenario 20C3M. . 14

3 Bulk measures of stability vs meridional temperature gradients. a) Dry stability vs surface meridional potential temperature gradient. b) Dry stability vs meridional potential temperature gradient at 500 hPa. c) Moist stability vs surface meridional equivalent potential temperature gradients. Each symbol represents one hemisphere and one season for one of the 20 models. Red=summer, blue=winter, green=fall, cyan=spring; O=Northern Hemisphere, X=Southern=Hemisphere. All units are K. See text for full definitions of stability and meridional gradients. . . . 15

4 SUPPLEMENTARY FIGURE 1. Change in saturated equivalent potential temperature (K) averaged over ocean only for the ensemble mean over all models, DJF (left) and JJA (right), scenario A1B minus scenario 20C3M. 16

5 SUPPLEMENTARY FIGURE 2. Change in moist stability (K), defined as the difference between the saturated equivalent potential temperature at 400 hPa and the surface equivalent potential temperature, between the A1B scenario and the 20C3M scenario, DJF (left) and JJA (right). 17

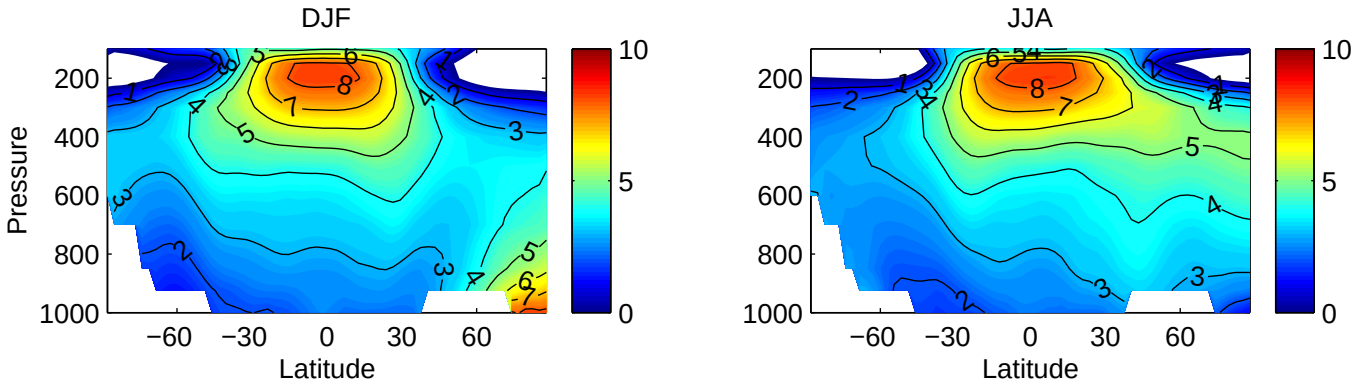

Figure 1: Change in potential temperature (K) for the ensemble mean over all models, DJF (left) and JJA (right), scenario A1B minus scenario 20C3M. Areas with mean cooling (in the polar stratosphere) are not colored.

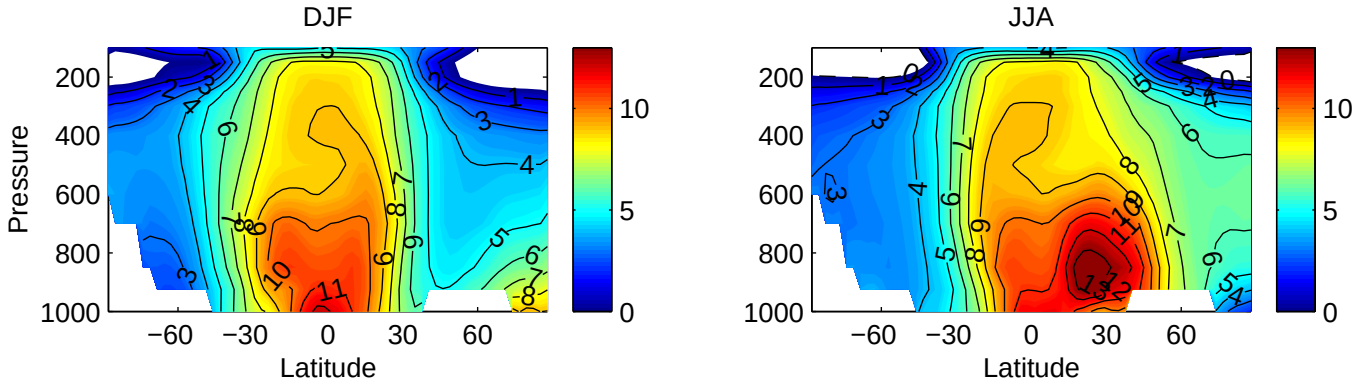

Figure 2: Change in saturated equivalent potential temperature (K) for the ensemble mean over all models, DJF (left) and JJA (right), scenario A1B minus scenario 20C3M.

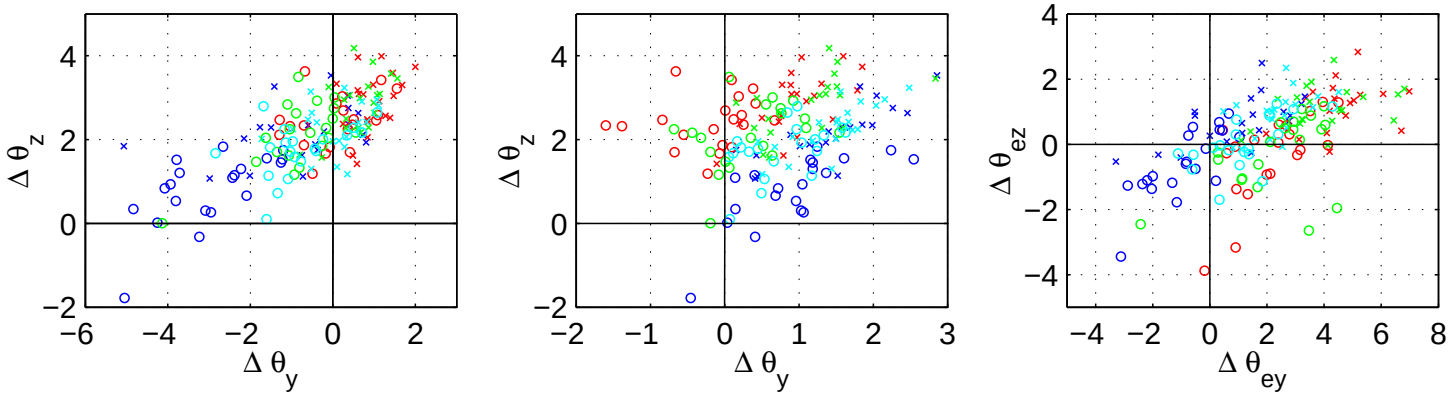

Figure 3: Bulk measures of stability vs meridional temperature gradients. a) Dry stability vs surface meridional potential temperature gradient. b) Dry stability vs meridional potential temperature gradient at 500 hPa. c) Moist stability vs surface meridional equivalent potential temperature gradients. Each symbol represents one hemisphere and one season for one of the 20 models. Red=summer, blue=winter, green=fall, cyan=spring; O=Northern Hemisphere, X=Southern=Hemisphere. All units are K. See text for full definitions of stability and meridional gradients.

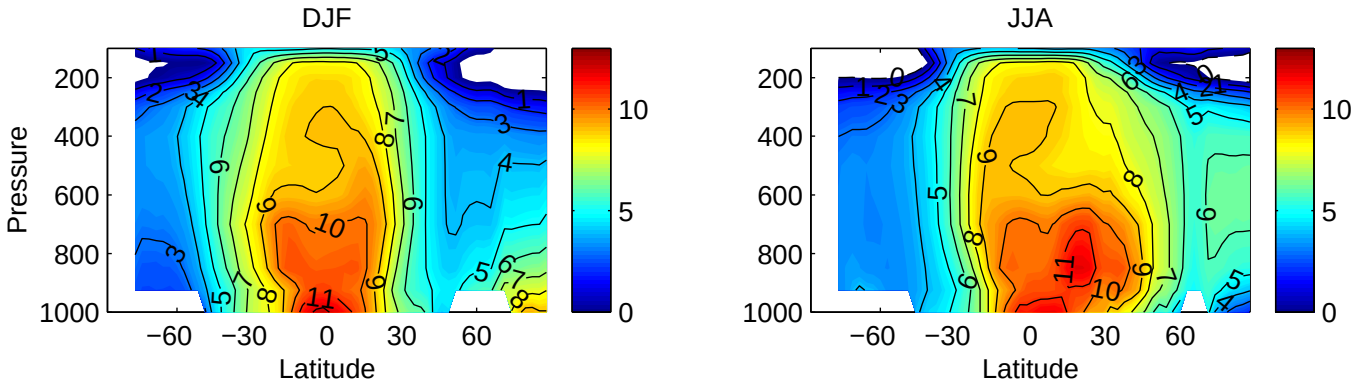

Figure 4: SUPPLEMENTARY FIGURE 1. Change in saturated equivalent potential temperature (K) averaged over ocean only for the ensemble mean over all models, DJF (left) and JJA (right), scenario A1B minus scenario 20C3M.

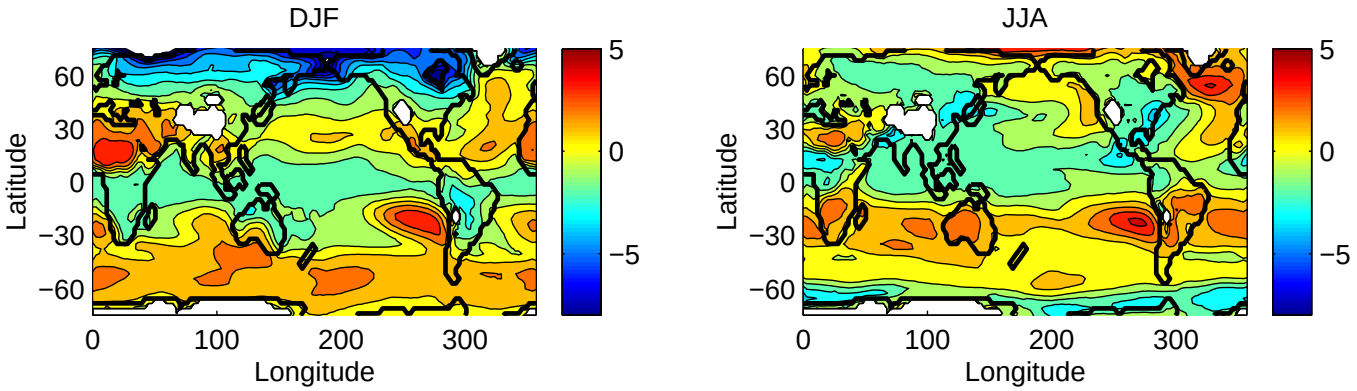

Figure 5: SUPPLEMENTARY FIGURE 2. Change in moist stability (K), defined as the difference between the saturated equivalent potential temperature at 400 hPa and the surface equivalent potential temperature, between the A1B scenario and the 20C3M scenario, DJF (left) and JJA (right).